ChemPubSoc Europe

DOI: 10.1002/open.201900007

Open Access ChemistryOPEN Reviews

Tips and Tricks for the Surface Engineering of Well-Ordered Morphologically Driven Silver-Based Nanomaterials

Roberto Nisticò,* Paola Rivolo, and Fabrizio Giorgis[a]

Particularly-shaped silver nanostructures are successfully applied in many scientific fields, such as nanotechnology, catalysis, (nano)engineering, optoelectronics, and sensing. In recent years, the production of shape-controlled silver-based nanostructures and the knowledge around this topic has grown significantly. Hence, on the basis of the most recent results reported in the literature, a critical analysis around the driving forces behind the synthesis of such nanostructures are proposed herein, pointing out the important role of surface-regulating agents in driving crystalline growth by favoring (or opposing) development along specific directions. Additionally, growth mechanisms of the different morphologies considered here are discussed in depth, and critical points highlighted.

1. Introduction

The term *"nanotechnology"* refers to the ability of creating reliable hierarchically-controlled engineered objects whose size is at the nanometer level (i.e., below 100 nm).[1–3] The comprehension of nanoscale phenomena (at the basis of the nanotechnology) is strictly correlated to surfaces and interfaces interactions involving the growing (solid) objects as well as the exploitation of these nanomaterials for advanced technological purposes due to their extremely peculiar properties.[4–6] Together with the human technological awareness, nanomaterials are becoming always much more important (and appealing) since continuously involved in many useful applications at the borderline between physics, chemistry, biology, medicine, materials science and engineering.[7–14]

According to the literature, there is a plenty of studies focused on the production of highly-ordered nanostructured (in)organic and hybrid/composite materials (and particles), whose architecture is driven by different synthetic methods and reaction mechanisms.[15–20] Among the different classes of nanomaterials, noble metallic nanoparticles (and other nanostructures) gain particular attention due to their catalytic, optical, electronic and magnetic properties exploitable in several multidisciplinary fields, such as catalysis, (nano)engineering for the production of optical and electronic/magnetic devices, drug-delivery systems, (bio)sensing, imaging, plasmonics, surface-enhanced Raman spectroscopy (SERS), biomedicine, and so on.[21–23] However, since the properties (and performances) of nanomaterials are strictly correlated to their size and morphology, a great effort was produced by worldwide researchers in order to reach well-controlled particular nanoscopic sizes and geometries, difficult to obtain by simple traditional methods.[21,24]

Within the last decades, much attention has been paid toward the production of shape-controlled metallic silver (Ag) nanostructures, mostly appealing in biomedicine (e.g., the familiar concept of *"silver care"* related to the well-known Ag antibacterial character) and for SERS analysis/sensing (i.e., due to their particular interaction with light at specific surface plasmon frequencies).[21,25–28] Interestingly, by varying some synthesis conditions, it is possible to produce silver nanomaterials according to different sizes and morphologies ranging from more conventional nanometric polyhedra and cubes,[29–30] (quasi)spherical systems,[31] planar sheets,[32] triangles,[33] to the more exotic nanostars,[34] nanoflowers,[35] nanodendrites,[36] nanometric nets and wires.[37–38] As reported in by Zhang *et al.*,[22] the thermodynamic and/or kinetic stabilization of the growing surfaces of the initial seeds of nanoparticles during the nucleation process drives the morphological evolution toward the desired nanostructures.

Actually, in literature plenty of different methods can be found for obtaining metallic nanostructures by using several structure directing agents (SDA) or templates and applying different experimental conditions (e.g., the type and concentration of reactants, environmental atmosphere, temperature, time, pH, and so on). However, due to the extremely high variety of conditions which affect the final nanostructure, the majority of the experimental approaches, followed by formulators, are mostly empirical and the resulting nanometric morphologies have been thereafter rationalized.

Therefore, aim of this review is to provide a valuable toolbox where researchers and formulators interested in the synthesis of particularly-shaped silver nanostructures can find useful guidelines and key-principles for setting up an aprioristic morphological design. In this context, growth mechanisms and driving forces behind the formation of particular nanostructures were discussed, providing a deep analysis of the scientific literature. Lastly, nanoengineering case studies were here presented, unveiling the role of all parameters involved in the

[a] Dr. R. Nisticò, Dr. P. Rivolo, Dr. F. Giorgis
Department of Applied Science and Technology DISAT
Polytechnic of Torino
C.so Duca degli Abruzzi 24, 10129 Torino, Italy
E-mail: roberto.nistico0404@gmail.com

considered syntheses. Obviously, for the sake of clearness it is important to notice that, since the scientific literature describing the synthesis of silver nanomaterials is extremely wide, we decided to consider as relevant only documents meaningful for this review comprehension and the subsequent discussion.

2. The Importance of Surface Science in the Growth of Metallic Nanostructures

As reported in the previous paragraph, the energetic stabilization of initial seeds surfaces, during the nucleation process, is the key-factor promoting the growth of some specific crystalline facets (rather than other ones) and thus driving the formation of peculiar nanostructures.[22]

Starting from the very basic concepts in materials science, crystalline materials (such as metals) can be organized into 7 crystal systems organized into 14 *Bravais* lattices, representing the primitive cell (i.e., the repeating crystalline units), each of them is defined by three edge length and three interaxial angles.[39] Silver, analogously to the other metallic elements forming the group 11 in the periodic table (namely, gold and copper), is organized according to the face-centered cubic (FCC) cell system, characterized by the basic crystal facets (100), (110), and (111). The surface energy (and consequently, the surface stability) of these flat crystal facets is following the order: $(111) < (100) \ll (110)$.[22] Moreover, the growth of high-index surfaces in these systems is possible only through the combination of terraces and steps of the previous three basic crystal facets allowable by the FCC crystal lattice. Figure 1A represents the process of formation of different surfaces. In detail, as reported by Zhang *et al.*,[22] {*hk0*} surfaces (in Figure 1A it is reported the (310) plane formation) is composed by a combination of (100) terraces and (110) steps, {*hkk*} surfaces (in Figure 1A it is reported the (211) plane formation) is composed by a combination of (111) terraces and (100) steps, whereas {*hhl*} surfaces (in Figure 1A it is reported the (221) plane formation) is composed by a combination of (111) terraces and (110) steps. More complex {*hkl*} surfaces, instead, can be obtained by a combination of terraces and steps of the basic facets with atomic kinks present at the junction points between them. By considering the surface energy of kinks, due to the lower coordination numbers they possess higher surface energies if compared to terraces and steps. In order to rationalize this knowledge, Figure 1B reports the strict correlation between the final morphology of the FCC silver crystal lattices and the surface atoms arrangements (in terms of terraces, steps, and kinks). In general, crystal lattices containing (100) facets yield cubic structures, those containing (111) facets often show octahedral ones, whereas the ones containing (110) facets favored the formation of rhombic dodecahedron structures. According to the surface energy scale $(111) < (100) \ll (110)$, the morphology related to the lower ones (namely, octahedral and cubic) are the most easily obtainable. Additionally, very complex morphologies can be reached combining the high-index crystal facets (see Figure 1B).

From this framework, it clearly emerged that the growth targeting of specific metallic facets rather than others is mandatory for obtaining exotic nanostructured morphologies,

Roberto Nisticò is Assistant Professor in Materials Science and Engineering at the Polytechnic of Torino (DISAT, Italy). He received his M.Sc. in Industrial Chemistry and his Ph.D. in Chemical and Materials Sciences both at the University of Torino (Department of Chemistry, Italy). His research is focused on several aspects at the interface between nanotechnology and materials science, always looking for novel and appealing solutions for a sustainable future. The principal, fields of interest are magnetic and/or metallic nanomaterials, functional/porous coatings, plasma treatments, biomaterials (for biomedical applications), valorization of natural resources, (bio) polymers and carbons, nanomaterials for photocatalysis and AOPs.

Paola Rivolo is a Research Technician at the Applied Science and Technology Department of Politecnico di Torino (Italy). In 1999, she obtained her Master's degree in Chemistry and, in 2004, her Ph.D. degree in Materials Science and Technology. Her research activities are mainly aimed at the surface chemical modification of porous and nanostructured materials for sensors and biosensors and, more recently, the application of metal-dielectric nanostructures integrated in optofluidic chips for SERS analysis in biodiagnostics. In particular, she recently started focusing on the synthesis and characterization of 3D silver-graphene hybrid aerogels chemically functionalized by macrocyclic molecules (e.g. porphyrins, phthalocyanines) and thiol-terminated oligonucleotides.

Fabrizio Giorgis is Full Professor in Experimental Physics of Condensed Matter at the Applied Science and Technology Department (DISAT) of Politecnico di Torino (PoliTo, Italy), where he is Deputy Director. He obtained his Master's degree in Physics in 1991 and his Ph.D. in Solid State Physics in 1995. His area of research concerns the synthesis and characterization of silicon-based thin films in amorphous/ microcrystalline/porous phases, 1D/ 2D/3D photonic crystals and metal-dielectric nanostructures with applications in photonic and plasmonic devices integrated in microfluidic platforms aimed to biosensing. In particular, most of his recent research is devoted to optical spectroscopy (fluorescence, FTIR, Raman/SERS) and photonic sensing devoted to the analysis of peptides, microRNA, aflatoxins in the frame of nanomedicine and precision agri-food.

thus altering the thermodynamic and the kinetic stability of the growing crystals. From the thermodynamic viewpoint, the shape of crystalline nanostructures will be dominated by surfaces parallel to the {*hkl*} planes (allowed by the crystal lattice) capable to guarantee low surface energy.[40] According to the Wulff's theorem, it is possible to apply an algorithm able to minimize the energy related to the crystal shape to the one concerning an outer surface energy, governed by the surface atomic lattice reconstruction. Indeed, the Wulff's theorem (reported in Figure 2)[41] graphically defines the crystal facets present in the selected nanostructure, by drawing a set of vectors from a common origin with length proportional to the surface energy along this orientation, constructing the planes perpendicular to each vector and finding the geometric structure having the smallest size with non-intersecting planes. According to the Wulff's construction theorem, the distance from the center to a specific surface of the crystallite is proportional to its specific surface free energy. Basing on this relation, crystal facets with higher values of surface energy grow faster thus forming surface areas smaller than those provided by the facets with lower surface energy.[22]

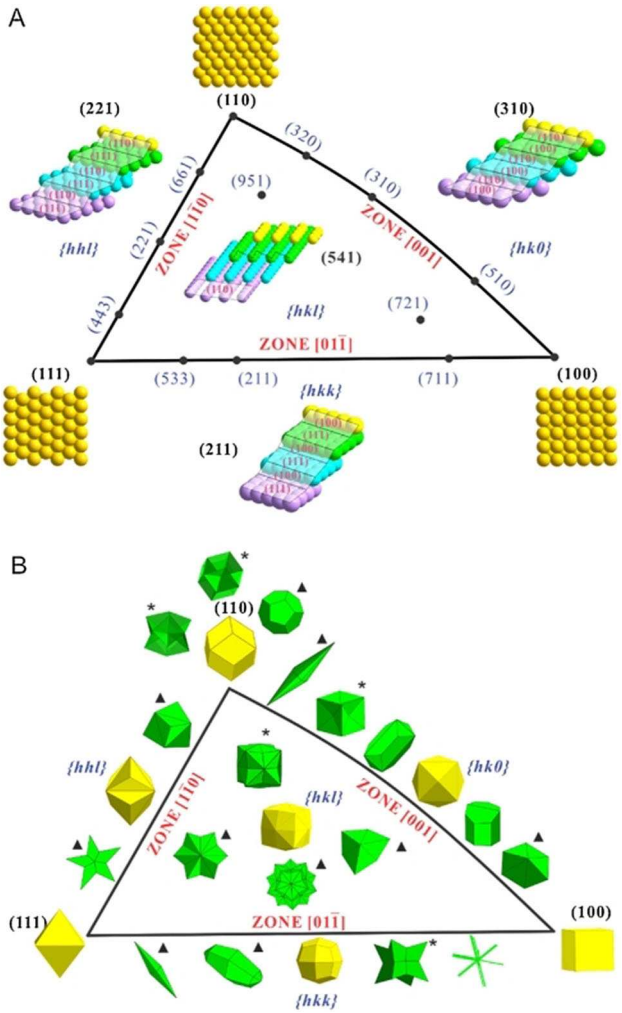

Figure 1. Surface atomic arrangements (A) and corresponding morphologies (B) of different crystal facets of FCC noble metal nanocrystals. In (B), the yellow models represent the common convex morphologies, whereas the green ones represent other unusual shapes, that may contain twin-plane (marked with a triangle) or concave feature (marked with a star). Reproduced with permission from Ref. [22]. Copyright (2016) Elsevier.

As a representative example, in Figure 3 the Wulff's construction rule is applied to the case of a hypothetical orthorhombic nanostructure with surface tension of planes (100) equal to (110) ones and to half of the (010) ones.[40] For this case study, the Wulff's theorem allows to define a rod-like prism equilibrium shape.

On the basis of the above discussion, by increasing the driving forces for crystallization, the final morphology of the metallic nanomaterial (e.g., silver) evolves from the simpler architectures (namely, polyhedrons and cubes, formed by the more thermodynamically stable low-index planes) toward hierarchically more complex nanostructures far-from-equilibrium (e.g., dendrites, as reported in Figure 4).[21]

Since the final morphology strongly depends on the micro/nanostructure formation condition in correlation to the thermodynamic equilibrium states, it is possible to modulate the growth of particular facets by altering their surface energies with the action of surface-regulating (or capping) agents.[22,42] The surface-regulating agents' method consists in the addition of chemical species, during the chemical (wet approach) synthesis, able to interact (mostly by adsorption mechanism) with a particular crystal face of the growing nanomaterials. By

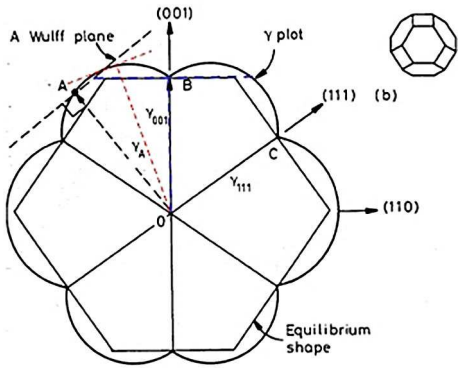

Figure 2. Wulff's construction theorem necessary for calculating the minimizing surface for a fixed volume with anisotropic surface tension. Reproduced with permission from Ref. [41]. Copyright (2011) The Authors.

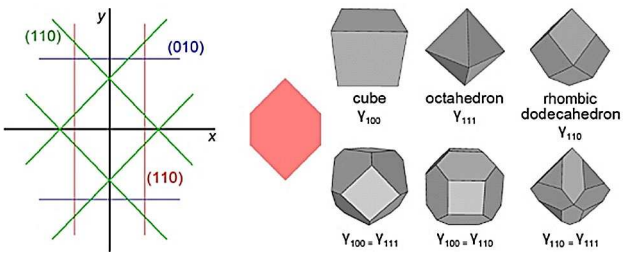

Figure 3. Example of Wulff construction for orthorhombic material. *xy* plane is parallel to the (001) plane of the material (left). Cross-section of the resulting equilibrium shape (middle). Some common Wulff constructions for materials with full cubic symmetry, such as FCC metals (right). The surface energies that have been used in the Wulff construction are shown below each shape. Reproduced with permission from Ref. [40]. Copyright (2015) The Authors.

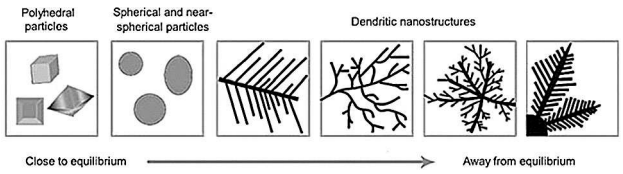

Figure 4. Correlation between the distance of the formation conditions from equilibrium and the morphologies of the formed metal nanostructures. Reproduced with permission from Ref. [21]. Copyright (2010) Elsevier.

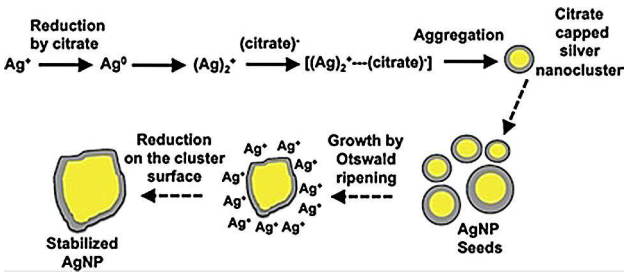

Figure 5. Schematic representation of the nucleation and growth mechanisms for AgNPs obtained by the citrate method. Reproduced with permission from Ref. [51]. Copyright (2004) American Chemical Society.

this way, it is possible to act directly on both the thermodynamics (by altering the surface energy of a particular facet) and the kinetics of the growing system.[43] Typically, these surface-regulating agents are classified into three main categories depending on the strength of interaction with the nanomaterial surfaces. They are: surfactants,[44] adsorbates,[45] and doping metal ions.[46] In the following paragraphs, the growth mechanism of silver nanoparticles (and other nanostructures) as well as the role of these surface-regulating agents will be discussed and, hopefully, clarified.

3. Growth Mechanism and Role of Surface-Regulating Agents

As reported by Marks *et al.*,[43] the main important nanostructures and the shape control induced on them by either thermodynamics or kinetics. In some cases, the same nanostructures are listed in both categories, but it has to be taken into account that all thermodynamically-stable nanostructures are obtainable also by applying a kinetic-control, whereas the opposite is not always valid. In order to unveil the thermodynamic and the kinetics factors affecting the growth mechanisms of these particular nanostructures, it is fundamental to clarify the different synthetic methods and the role of the surface-regulating agents.

In general, the methods used for the preparation of metal nanoparticles can be grouped into two different categories: namely, either the top-down or the bottom-up approach.[18,47] In the former, the nanoparticles are obtained starting from bulk materials, in the latter molecular precursors are involved.

Actually, the literature related to the synthesis of Ag nanostructures is very wide, in this study only wet chemistry approaches were considered. In general, wet chemical methods usually employ three main components in the batch solution: i) the metal precursors (usually metal salts), ii) the reducing agents, and iii) the stabilizing/capping agents (for details, *vide infra*). Among the different chemical methods to produce silver nanoparticles, the citrate-mediated (or Turkevich) synthesis[48–49] and sodium borohydride reduction of silver cations[50] are the most largely reported in the literature. In detail, the Turkevich method (initially relies on the synthesis of gold nanoparticles from $AuCl_4^-$, then extended also to the production of other metals)[47] consists in reducing metal cations in aqueous medium, nearby the boiling point, in presence of trisodium citrate dihydrate. As depicted in Figure 5,[51] the role of citrate compound is twofold: on one side, it acts as reducing agent of the metal cation (from Ag^+ to Ag^0), whereas on the other side, the reactant works as stabilizing agent of the growing nanometric structures. According to the mechanism proposed in Figure 5, once the first metallic seeds are obtained from the Ag^+-to-Ag^0 reduction, the remaining citrate anions start to give complexation phenomenon at the silver surface, thus decreasing significantly the number of citrate species still available in solution (and necessary for reducing the residual silver cations). Following such mechanism, few seeds grow up via Ostwald ripening mechanisms,[52] which consists in the growth of larger particles by consuming the smaller ones. As a consequence of the high time necessary for completing this citrate-mediated reduction reaction (slow rate), large nanoparticles (in the 50–100 nm range) are produced, exerting a size-control action.

On the contrary, the sodium borohydride reduction mechanism of silver consists in exploiting the reducing action of $NaBH_4$ at relative low temperature (nearby room temperature, RT) following the chemical pathways proposed in Equation (1):

$$M^{n+} + nBH_4^- \rightarrow M^0 + nB(OH)_3 + n3.5H_2 \quad (1)$$

The formation of AgNPs is based on the temporary stabilization action of the AgNPs by the excess of borohydride species, whereas the collapse of the stabilization is due to the proliferation of aggregation phenomena due to the consumption of borohydride species by hydrogen evolution,[50] according to the chemical mechanism reported in Equation (2):

$$BH_4^- + 4H_2O \rightarrow B(OH)_4^- + 4H_2 \quad (2)$$

In this case, the particle growth mechanism can be organized into four steps (Figure 6). It consists in an initial step

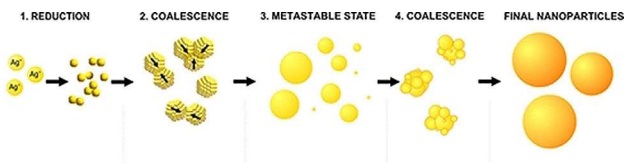

Figure 6. Schematic representation of the four-step growth mechanism for AgNPs obtained by the borohydride method. Adapted with permission from Ref. [50]. Copyright (2012) American Chemical Society.

where the rapid reduction of the silver precursor takes place followed by a primary coalescence step where the reduced silver atoms generate dimers and other oligomers (clusters). Afterwards, this coalescence phenomenon proceeds until the final particles have a diameter of ca. 5–6 nm. At some point of the synthesis (denoted as switching point), a strongly decrease of the colloidal electrostatic stability of particles occurs (correlated to the hydrolysis of borohydride as shown by Equation 2). This favors further coalescence phenomena, which are responsible for the formation of small nanoparticles, sized in the range of ca. 10–20 nm, and thus remarkably small if compared to the ones obtained by the Turkevich approach (*vide infra*).[50] This size-control is due to several factors among which the most relevant ones are: (i) the coalescence-driven growth mechanism due to the action of borohydride anions (that is different if compared to the citrate-mediated one), and (ii) the synthesis process at low temperatures.

Apart from these two species (namely citrate and borohydride), in the literature several other chemicals able to promote the reduction of Ag cations into metallic silver (e.g., ascorbic acid, gallic acid, hydrazine, hydroquinone, humic-like substances, polyols, etc.). As suggested by Pacioni and co-workers,[47] the key-factor is the matching of the redox potential of silver cations in water (Ag^{+}-to-Ag^{0} reaction, $E^{0} = +0.799$ V), with the one of the reducing agents, taking into account that the final ΔE^{0} must be positive ($\Delta E^{0} > 0$).

The promotion of facets growth along a selected direction can be achieved by the surface-regulating agents (namely, surfactants, adsorbates, or metallic ions).

Surfactants are amphiphilic molecules where hydrophilic functionalities (head) are bonded with hydrophobic ones (tail). However, this is the standard definition, since several further (and more complex) chemical structures showing amphiphilic properties are possible (e.g., humic substances, (co)polymers, crown ethers, and so on).[53–56] According to the hydrophilic functional groups, they can be classified as ionic (charged) or non-ionic (polar uncharged) surfactants. Due to their peculiar structure, they can self-organize themselves into supramolecular aggregates (micelles), able in preventing the aggregation phenomena but also exploitable in soft-templating processes.[18,57] As previously discussed, such molecules can also weakly interact with the surface of some specific facets of the growing crystallites. As an example, in their recent work, Sun *et al.*[58] demonstrated that by modulating the ratio between Ag cations and the capping agent polyvinylpyrrolidone (PVP), at 110 °C, in presence of ascorbic acids (as reducing agent), it is possible to favor the growth of nanorods by extending the {111} facets from multiply twinned particles (MTPs) with a decahedral shape during the early growth stages. In fact, as depicted in Figure 7, MTPs present 5-fold symmetry (characterized by having ten {111} facets). The further crystallization of silver atoms on the MTPs leads to the uniaxial elongation along with the confinement of twin planes (labeled in red), thus forming rod-shaped nanostructures. Interestingly, PVP tends to preferentially adsorb (by means of the O and N atoms of the PVP units) to the newly formed side surfaces of the {100} facets, rather than the {111} facets, which continue to attract silver

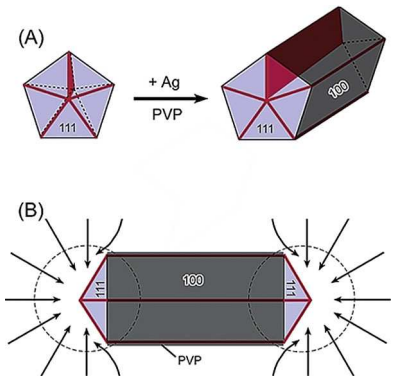

Figure 7. Schematic illustration of the mechanism proposed to account for the growth of silver nanowires with pentagonal cross sections. A) Evolution of a nanorod from a multiply twinned nanoparticle (MTP) of silver under the confinement of five twin planes and with the assistance of PVP. The ends of this nanorod are terminated by {111} facets, and the side surfaces are bounded by {100} facets. The strong interaction between PVP and the {100} facets is indicated with a dark-gray color, and the weak interaction with the {111} facets is marked by a light-blue color. The red lines on the end surfaces represent the twin boundaries that can serve as active sites for the addition of silver atoms. The plane marked in red shows one of the five twin planes that can serve as the internal confinement for the evolution of nanorods from MTP. B) Schematic model illustrating the diffusion of silver atoms toward the two ends of a nanorod, with the side surfaces completely passivated by PVP. This drawing shows a projection perpendicular to one of the five side facets of a nanorod, and the arrows represent the diffusion fluxes of silver atoms. Reprinted with permission from Ref. [58]. Copyright (2003) American Chemical Society.

atoms during the growth.[58] Moreover, a higher PVP content favors the isotropic coverage of the growing nanoparticles, without giving a preferential stabilization and thus producing spherical-shaped nanostructures.[59] Analogous results are also obtained by means of cetyltrimethylammonium bromide (CTAB) as surfactant, for the production of gold nanorods.[60]

The second surface-regulating agents known as adsorbates, are typically small molecules (such as CO, NO_2, (organo)amines, halides, etc.) able to strongly interact with specific crystal surfaces on metallic nanoparticles. Different adsorbates stabilize different facets.[22] For instance, concave octapod Pt metallic nanoparticles with high-index {411} facets are prepared by Huang and co-workers[61] in presence of PVP and methylamine. The role of methylamine consists in a selective binding to the high-index {411} facets of Pt during the crystallite growth. By performing the same synthesis in absence of the capping agent, mixed morphologies are obtained (mostly, cubes and octahedral), thus confirming the morphological driving action of the adsorbate species. In their study, Gomez-Grana *et al.*[45] have studied the effect of chlorides compounds in stabilizing the {100} facets of Ag. In detail, the Ag shell deposition on Au seeds (i.e., core@shell: Au@Ag) with variously defined structures was studied. A growth mechanism in which the final morphology is achieved by means of kinetically-controlled surface stabilization of the {100} facets by halides adsorption was proposed. Figure 8 reports the theoretical simulation of the chlorides adsorption on Au facets with different orientations coated with two monolayers of Ag (111), (100), and (110). The results evidence that Cl atoms are prone to the interaction with Ag on the (111)

facets, but are favored to form denser structures with the (100) facets due to a stronger interaction. The experimental data support the peculiarity of chlorides to adsorb on Au@Ag nanoparticles thus allowing the achievement of architectures rich in {100} facets.

Lastly, the use of foreign metallic ions as surface-regulating agents for the production of controlled-shape metallic nanoparticles, by means of underpotential-deposition (UPD) processes via alloying reactions, gained much attention.[46,62–64] UPD processes consist in foreign metal deposition on metallic substrates at positive potentials with respect to the Nernst thermodynamic prediction (in fact, usually metal deposition involves overpotential deposition phenomena). The main advantage of this UPD process is the high degree of precision and rapidity. Conversely, this technique has the main drawback to be limited to the deposition of metal nanostructures following the galvanic (electropotential) series, which determined the "nobility" of metals.[62] Bokshits *et al.*[63] reported the UPD deposition of lead on silver, gold, and bimetallic silver/gold colloids. Xia and co-workers,[46] instead, describe the influence of copper ions in favoring the preferential growth of Ag nanocubes seeds along $<111>$ directions, thus evolving into more elongated structures (namely, from concave cube to octapods). Vice versa, when silver is not considered in terms of bulk metallic nanostructures, but as foreign metal ions, e.g., in the case of a core-shell Au–Ag system, it is possible to stabilize either the {110} facets or the high-index {310} and {720} facets, by varying the amount of silver ions in solution.[64] Figure 9 reports the four different morphologies (namely: octahedra, rhombic dodecahedra, truncated di-tetragonal prisms, and concave cubes) obtained by means of the UPD of silver along with the increase of Ag^+ in solution.

Additionally, concerning the use of surface-regulating agents, it is worth noticing that the Wulff's construction theorem is applied under thermodynamic equilibrium conditions, whereas, in most cases, the growth of metallic nanostructures also happens under non-equilibrium conditions, strongly influenced by the supersaturation (which is the difference between the chemical potentials of the metal atoms in solution vs. the potentials of the metal bulk nanomaterial). Such supersaturation conditions affect the kinetics of the nucleation process, thus allowing to obtain high surface energies architectures, since the higher the metal reduction rate, the higher the supersaturation. As highlighted by Zhang *et al.*,[22] by increasing the mixing rate during the synthetic process, an augmented reduction rate can be achieved (due to the higher concentration of metal precursors in the solution). Moreover, also the introduction of additives (such as pH-controlling agents) is able to favor the reduction ability of the reducing agents. In fact, it has been monitored the evolution from low-energy {100} Au nanocubes to high-energy {110} Au rhombic dodecahedra by addition of strong bases to enhance the reduction ability of ascorbic acid.[65]

Clearly, the discussion concerning the applicable alternative and various procedures could be a not trivial task in terms of the clear and concise rationalization of the huge amount of literature sources. For this reason, in this work we considered only the wet-chemical approaches. However, for the sake of completeness, it is worth noticing the physical (i.e., physical energetic sources, such as arc discharge, thermal treatments, etc.),[66] electrochemical (consisting in a metallic dissolution at

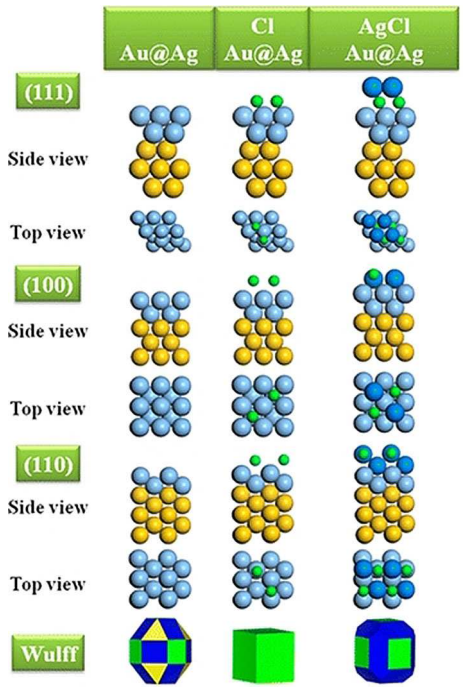

Figure 8. Calculated surface structures for different facets: (111), (100), (110), and different surface terminations. Left column: two silver monolayers on gold Au@Ag(2 ML); central column: Cl adsorption in a dense phase; right column: AgCl growth on Au@Ag(2 ML). In each case, the termination of AgCl follows that of the substrate. Color code: golden Au, blue Ag, dark blue Ag^+, green Cl atoms/ions. The bottom row shows the corresponding Wulff (equilibrium) structures: yellow planes are {111}, green planes are {100}, and blue planes are {110} facets. Reprinted with permission from Ref. [45]. Copyright (2013) American Chemical Society.

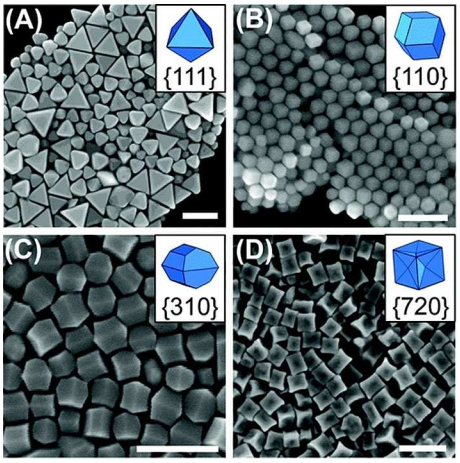

Figure 9. SEM images of A) octahedra, B) rhombic dodecahedra, C) truncated di-tetragonal prisms, and D) concave cubes synthesized from reaction solutions containing Ag^+/Au^{3+} ratios of 1:500, 1:50, 1:12.5, and 1:5, respectively. Scale bars: 200 nm. Note that the octahedra form concomitantly with {111}-faceted twinned truncated bi-tetrahedra, which are larger in size. Reprinted with permission from Ref. [64]. Copyright (2011) American Chemical Society.

the anode and a subsequent metal reduction at the cathode by means of the current density adjustment),[67] photochemical (where the chemical mechanism is induced by light sources),[68] and biological (i.e., the exploitation of reducing/stabilizing agents produced by living organisms, such as bacteria, fungi, or plants extracts)[69–70] methods exploitable for the production of metallic nanomaterials with specific morphologies.

The following paragraphs are devoted to the analysis of different case studies selected from the scientific literature. Particular attention will be paid to the production of several obtainable exotic nanoscopic morphologies and a particular emphasis will be given to the role of the experimental parameters and chemicals in driving the synthesis toward unusual geometries.

4. Surface Engineering Applied to Exotic Morphologies: Metallic Silver Case Studies

According to what has been previously discussed, metallic silver atoms tend to self-organize in the FCC cell system, characterized by the basic crystal facets (100), (110), and (111). As reported in Figure 1, crystal lattices containing either (100) or (111) facets allow obtaining nanocubes or octahedra respectively, whereas lattices containing (110) facets only favor the formation of rhombic dodecahedra. Due to the surface energy scale $(111) < (100) \ll (110)$, cubic and octahedral systems are the most easily obtainable, immediately followed by the (110)-derived rhombic dodecahedral ones. However, the literature is full of studies reporting the synthesis of different morphologies (such as, spherical systems, planar sheets, triangles, etc.) as well as more exotic architectures (e.g., nanostars, nanoflowers, nanodendrites, nanometric nets and wires). The cited unusual and exotic morphologies will be reviewed in the following subparagraphs by focusing the literature case studies which describe the wet chemistry synthesis of silver nanomaterials.

4.1. Triangular Plates

In those years, triangular silver nanoplates (or nanoprisms) are produced by means of several methods. In their study, Wang *et al.*,[71] report the synthesis of silver nanotriangles from silver nitrate in dimethylformamide (DMF) refluxed at 140 °C for ca. 4 hours in presence of PVP as capping agent. Xue and co-workers,[72] instead, produce silver nanotriangles starting from silver nitrate and trisodium citrate aqueous solution in presence of $NaBH_4$ and NaOH (injected dropwise). In detail, nanotriangles are produced by a 70 W sodium lamp irradiation for 2 hours. This photochemical approach has been classified as plasmon-mediated method since light radiation favored the surface plasmon resonance of the AgNPs, thus catalyzing the citrate-induced reduction of silver ions onto the AgNPs, so driving the growth of triangular-shaped systems. At the same time, a slight oxidation occurs of the small spherical seeds of AgNPs induced by the oxygen dissolved in water to form silver ions. Analogous results were also obtained by Jia *et al.*.[73] Wijaya *et al.*[33] report the synthesis of triangular silver nanoplates in presence of PVP, polyacrylamide (PAM) and/or acetonitrile at 80 °C for one day. Figure 10 shows the silver nanostructures obtained at different experimental conditions. Figure 10A reports that the AgNPs, obtained by maintaining the weight ratio PVP/$AgNO_3$ equal to 19.5 in absence of both PAM and acetonitrile, are quasi-spherical, thus indicating the growth of the more thermodynamically favored decahedral structures. Conversely, by introducing PAM (i.e., weight ratio PAM/$AgNO_3$ equal to 0.098) into the solution, some triangular nanosystems (average length ca. 100 nm) started growing together with the presence of smaller quasi-spherical NPs (Figure 10B). The addition of PAM affects the reduction rate and so promotes the formation of the triangular systems. By introducing also the acetonitrile (0.019 M acetonitrile concentration), a significant increment of the smaller triangular systems (average length ca. 70 nm) is reached (Figure 10C). Furthermore, a synthesis which involves PVP and acetonitrile only (PAM is not added) leads to the formation of few silver triangular systems only (Figure 10D). By this study, the authors determined that: i) synergistic effects of both PAM and acetonitrile take part to decrease the reduction rate and consequently to favor the formation of triangular systems thus promoting a kinetic control of the reaction, and ii) higher/lower PVP:$AgNO_3$ ratios favor the formation of larger/smaller triangular geometries.

Li and co-workers[74] studied the production of metallic silver triangular plates in presence of PVP (as capping agent) and hydrazine (as reducing agent). In this study, the growth of triangular nanoparticles is kinetically-driven by the PVP selective-interaction with (111) growing facets during the Ostward ripening process. Lastly, Zhang *et al.*[75] reported that H_2O_2 can favor the formation of silver triangular nanoplates by means of etching reactions in presence of PVP, trisodium citrate and sodium borohydride. As shown in Figure 11, if PVP is added separately, quasi-spherical silver nanoparticles are produced (Figure 11B). Conversely, by introducing H_2O_2, a promotion of

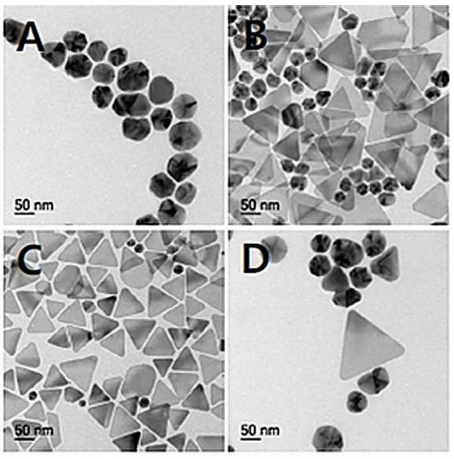

Figure 10. TEM images of Ag nanoplates formed in a water medium A) in the absence of PAM and acetonitrile and in the presence of B) PAM, C) PAM and acetonitrile, and D) acetonitrile. Reprinted with permission from Ref. [33]. Copyright (2017) Royal Society of Chemistry.

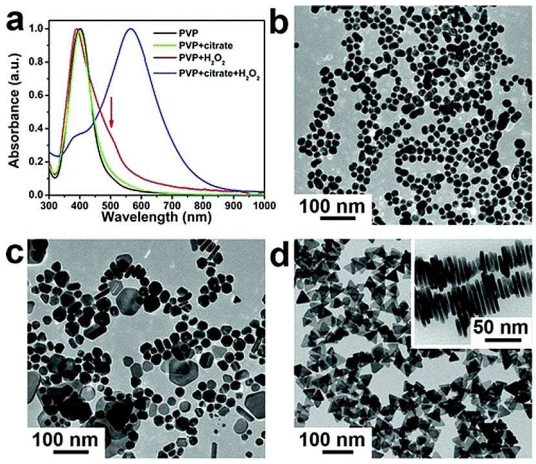

Figure 11. a) UV/Vis spectra of silver nanoparticles synthesized under different conditions. TEM images showing the morphology of products prepared in the presence of b) PVP only, c) PVP and H_2O_2, and d) PVP, citrate, and H_2O_2 together. The inset in (d) shows a TEM image in which Ag nanoplates stand vertically upon their edges. Reprinted with permission from Ref. [75]. Copyright (2011) American Chemical Society.

anisotropic structures is obtained (with formation of spherical, rod-like and plate-like NPs, Figure 11C). The addition of citrate in the PVP and H_2O_2, instead, favor the formation of homogeneous triangular nanoplates (Figure 11D). Moreover, on the basis of further experiments, the authors explain the synergic role of citrate and H_2O_2: on one side, citrate molecules

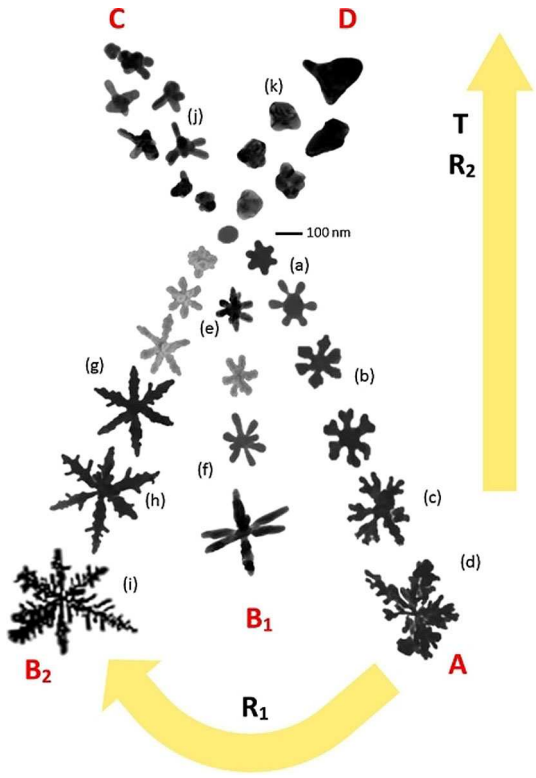

Figure 12. Growth pathways determining the different mechanisms of nanostar synthesis deduced from the analysis of the TEM and SEM images. Reprinted with permission from Ref. [34]. Copyright (2017) Elsevier.

preferentially bind to (111) facets, on the other side, H_2O_2 favors the consumption of the less-stable AgNPs by oxidizing them to Ag^+. This way, the growth of the side (100) facets, which form triangular plates, is favored but if the concentration of H_2O_2 is increased, Ag plates can be completely etched.[76] Thus, for such systems, a delicate balancing between reduction (by the reducing agent borohydride) and oxidation (due to the etching agent H_2O_2) must be properly maintained.

4.2. Branched Nanostructures

Due to the increasing interest on systems yielding localized surface plasmon resonances, nanometric star-shaped silver nanoparticles catch the attention of worldwide researchers. In particular, the presence of sharp tips within such nanostructures are able to carry out "hot spot" effects concerning surface-enhanced Raman scattering (SERS), provoking huge Raman enhancements in nanometer sized areas.[23,77–78] In the study written by Garcia-Leis *et al.*,[34] it is reported the production of silver nanostars by chemical reduction of silver ions in presence of both hydroxylamine (HA, first step) and citrate (CIT, second step). Basically, three parameters are tuned: (i) the [HA]/[Ag^+] ratio (R1), (ii) the [HA]/[CIT] ratio (R2), and the time between reduction reactions (T). Figure 12 reports the analysis of the obtained morphologies. Hexagonal (or six-branched) symmetric nanostars (Figure 12, line A) can be synthesized at low T, R1, and R2, giving rise to the formation of dendrites. Octahedral (or eight-branched) symmetric nanostars with either smooth arms (Figure 12, line B1) or snowflakes-like dendrites (Figure 12, line B2) can be obtained by increasing the parameter R1. On the contrary, by increasing both T and R2, and maintaining high R1 value, it is possible to get irregular (generally four-branched, with long and short arms) nanostars (Figure 12, line C), whereas undeveloped nanostars (without any protrusions formation) can be obtained for low R1 values (Figure 12, line D). The suggested mechanism defines the initial (hydroxylamine-driven) formation of the low energetic (100) cubic and (111) octahedral seeds, followed by a second (citrate-driven) step where the formation of hexagonal (from nanocubes) and octagonal (from octahedral systems) nanostars takes place. Experimental results evidence that the most important parameter is the [HA]/[Ag^+] ratio (R1), which driven the formation of either octahedral or nanocubic seeds, thus governing subsequently the growth of either eight or six branched stars. On the contrary, both the [HA]/[CIT] ratio (R2) and time between reduction reactions (T) are negative parameters, since they influence the homogeneity (reducing it) as well as the formation of branched structures.

A simple and more environmental-friendly approach for the production of branched Ag (coral-like) nanostructures is reported by Wang *et al.*,[79] where L-ascorbic acid is used as reducing agent. Figure 13 reports the concentration effect of L-ascorbic acid, where the silver ions one is maintained at a fixed value. The acid concentration is varied in the range from 0.23 to 4.6 mM. Results evidence that at low concentration of L-ascorbic acid, irregularly-faceted silver particles without branches are obtained, probably due to the low reduction rate

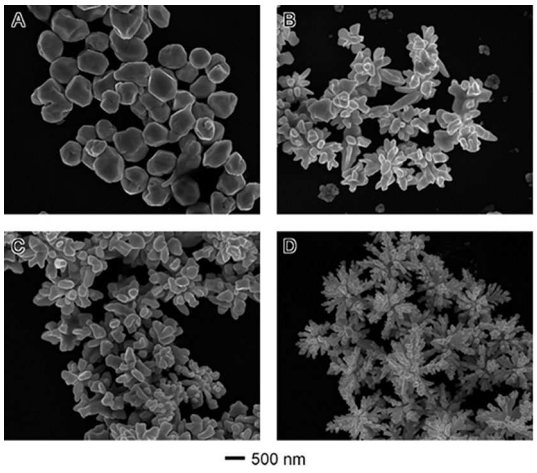

Figure 13. SEM images showing the effect of L-ascorbic acid concentration on the particle morphology. The L-ascorbic acid concentrations were: A) 0.23, B) 0.46, C) 0.93, and D) 4.6 mM. The concentration of $AgNO_3$ was 0.23 mM for all reactions. The reaction times were 20 min. Reprinted with permission from Ref. [79]. Copyright (2008) American Chemical Society.

(Figure 13A). On the contrary, by increasing the L-ascorbic acid concentration, branched structures are achieved (Figure 13B, 13 C, and 13D). This is probably due to the favorable formation of the seeds with the proper geometry. In general, higher L-ascorbic acid concentration values favor the formation of longer and ramified branches.

Interestingly, Lou and co-workers[80] produced 2D gear-like silver nanostructures by using both citrate and L-ascorbic acid. As demonstrated by the authors, long seeding period (the time between citrate and L-ascorbic acid addition) reduces the size of the formed seeds, and high concentration of L-ascorbic acid decreases the size of the final crystals. It seems that there is a synergism between citrate and ascorbic acid: the former works as shape-directing agent (by adsorbing preferentially onto the (111) facets), while the latter acts as reducing agent. Jena *et al.*,[81] instead, produce branched flower-like Ag nanostructures by using rutin as reducing/capping agent. The mechanism proposed by the authors relies on the initial formation of small spherical metallic seeds (instead of the cubic/octahedral systems previously described) followed by the initial formation of anisotropic short-branched NPs, probably generated by the preferential growth of (111) crystal planes (in agreement with the other analyzed case studies). The growth of such branched nanostructures strongly depends on the concentration of rutin (which probably defines not only the Ag reduction rate, but also the preferential growth). Furthermore, Qingquan *et al.*[35] reported the synthesis of silver nanoflowers by using L-cysteine as reducing agent. The most relevant finding consists in the assessment of the molecular ratio between L-cysteine and the metallic silver precursor as main critical parameter of the synthesis. In fact, since this is a seed-mediated process, low cysteine/silver molecular ratios produce few unstable seeds which are not able to evolve into flower-like systems.

Lastly, Zhang and co-workers[82] produce hierarchical flower-like silver particles by using ascorbic acid as reducing agent, PVP and different organic acids (e.g., citric acid, malic acid, and oxalic acid) as structure-directing agents. As reported in Figure 14, different textured topographies (defined by different shapes and sizes) are obtained by changing the structure-directing agent. In detail, in absence of any organic structure-directing agents, spherical (1–2 μm sized) particles made of irregular strips were achieved (Figure 14a). Moreover, the addition of citric acid in the synthesis slurry, favors the growth of spherical particles formed by the radial organization of nanorods (Figure 14b). Malic acid, instead, leads to the formation of metallic walnut-like morphologies with spherical contours (Figure 14c), and finally oxalic acid allows to obtained spheroidal particles made of cross-linked silver nanosheets (Figure 14d). The authors proposed a growth mechanism consisting in the initial formation of complexes between the negatively-charged carboxylic acids functionalities of the organic acids and the positively-charged silver cations present in the solution, followed by the reduction by action of ascorbic acid of silver ions released from the complexes. Once seeds are formed, they start growing by capturing the metal ions from the solution. This route is a kinetically-controlled process driven by the organic acids concentration (which consequently guides the ions release/reduction). Interestingly, it has been demonstrated also that high temperatures speed up the process (influencing the reduction rate), thus favoring an "undesired" isotropic growth.

4.3. Nanometric Silver and the Filamentous Growth

Quite recently, the high interest about optoelectronic and magnetic devices attracted much attention of worldwide researchers on the development of 1D metallic nanomaterials, such as nanorods, nanowires, and nanonets, thus becoming a fascinating subject of research.[83–84] In their comprehensive analysis, Zhang and co-workers[44] analyze previous works concerning the production of silver nanowires, with a particular emphasis on the different synthetic alternatives. According to them, the polyol method is the easier procedure for obtaining

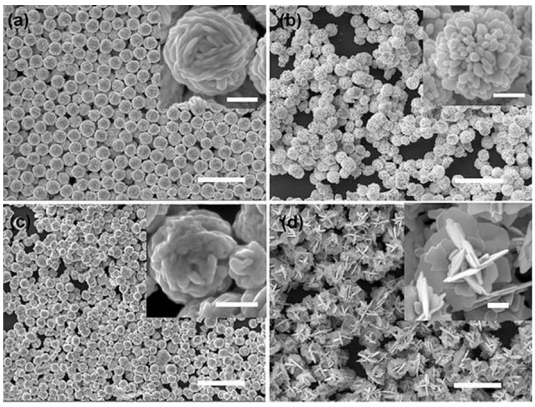

Figure 14. SEM images of hierarchical flower-like Ag nanostructures without (a) and with organic acids, such as citric acid (b), malic acid (c), and oxalic acid (d). The scale bars are all 5 μm, while the insets ones are 500 nm. Reprinted with permission from Ref. [82]. Copyright (2017) Springer.

silver nanowires.[44] Typically, PVP is introduced in the synthesis for favoring the growth of elongated architectures.

In their study, Chen *et al.*[84] report the production of silver nanorods from silver nanowires by means of a polyol process based on PVP as capping agent and ethylene glycol (that is the polyol) as solvent/reductant. It consists in a three-step process, where: in the first step, the formation of Ag nanoparticles seeds occurs; in the second step, the formation of nanowires takes place by means of PVP; finally, in the third step, the growth of such nanowires, evolving into silver nanorods is obtained. Figure 15 reports the morphological evolution of 1D nanomaterials from wires to rods. In detail, the nanowires in Figure 15A are formed following the same growth mechanism previously reported in Figure 7, thus resulting in structures characterized by pentagonal cross-section with side {100} surfaces and transversal {111} ones. On the contrary, after a purification step (PVP is substantially removed), in the third step (the wires-to-rods evolution) of the process a significant radial growth (thickening) predominates over the axial growth (elongation). This axial growth is diminished because of the growth of the {100} surfaces due to silver ions adsorption faster than the one of {111} surfaces, without the protective action of PVP. Additionally, authors report that if extra-PVP is furtherly added at the third step, the radial growth is significantly diminished since PVP preferentially interacts with the lateral {100} surfaces.

As reported in Zhang *et al.*,[44] the main factors influencing the preferentially axial growth are: the temperature (low temperatures decrease the reducing power), reaction time, PVP concentration (higher content of PVP, shorter nanostructures are obtained) and molecular weight (the longer the PVP chains, the longer and thinner the wires structure), Ag salts concentration (higher Ag salts concentration favors the production of shorter and thicker structures), the PVP:Ag salts ratio, the use of other surface-regulating agents, and so on.

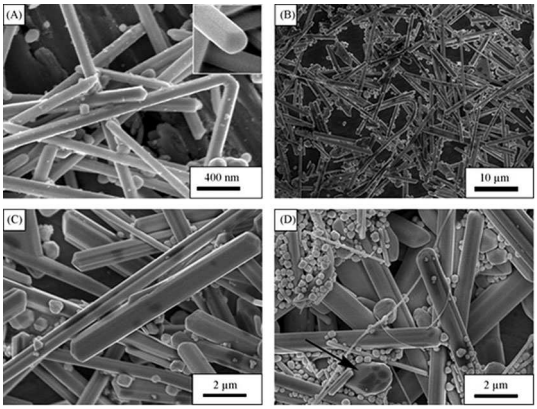

Figure 15. SEM images of silver nanowires and nanorods. A) Purified silver nanowires synthesized in step 2, which act as the seeds in step 3, the inset image shows the pentagonal cross section. B) Silver nanorods synthesized by using purified silver nanowires as seeds, the mole ratio of PVP/$AgNO_3$ is 0.5 and concentration of $AgNO_3$ is 1.0 M; C) magnified 10 times of (B); D) silver nanorods synthesized with the mole ratio of PVP to $AgNO_3$ is 1.0, and other conditions are the same as (B); the black arrow shows the polygonal cross section of nanorods. Reprinted with permission from Ref. [84]. Copyright (2008) Elsevier.

Lee *et al.*[85] report the production of silver nanorods by seed-mediated growth (produced by borohydride-mediated reduction in presence of citrate). Nanorods were produced by using ascorbic acid as reductant and CTAB as surface-regulating agent. It has been found that during growth of nanorods, CTAB forms a bilayer structure around them.[86] Furthermore, it is demonstrated that the increment of both temperature and pH causes an increment of the silver reduction rate, thus favoring the growth of short monodisperse rods particles. Interestingly, by changing the surfactant counterions (from bromide to chloride), more spherical structures are produced, probably because also chlorides influence the capping action of the cationic surfactant (chlorides preferentially adsorb on (111) faces).[87] The role of inorganic ions in orienting the growth of particular structures relies on the Hofmeister series, in accordance to our previous studies.[20,88]

Lastly, Lee and co-workers[89] report the production of silver nanonets due to the assembly of silver spherical/peanuts-shaped nanoparticles. The mechanism proposed in Figure 16 is based on the non-uniformity of the surface charges distribution between the primary particles. This phenomenon allows the NPs to assemble forming a nanonet.

5. Conclusions and Future Remarks

Nanotechnology is a fascinating scientific field which, since its very beginning, has opened new future scenarios and unique technological opportunities. Even if, in most cases, the exact role of all components in the growth mechanisms of metal nanostructures is still unclear, the knowledge development about this topic is significantly growing during the last years. In this context, the progress in the field of optoelectronics and sensing surely will give a significant boost in developing processes for the production of metallic nanomaterials (i.e., silver based), able to guarantee a much higher degree of morphological control. Through the text, the main relevant principles behind the surface engineering (i.e., basically the surfaces stabilization) were discussed, with particular attention to the factors influencing the final morphology. It has been demonstrated that the Wulff's construction theorem is able to unveil how particular morphologies are obtained. By consider-

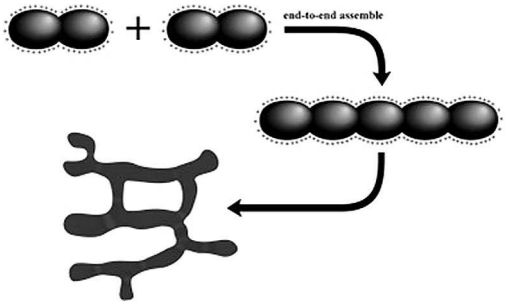

Figure 16. Schematic illustrations of the Ag nanonets formed by an end-to-end assembly of Ag nanopeanuts. Reprinted with permission from Ref. [89]. Copyright (2010) Elsevier.

ing metallic silver, it has been demonstrated that morphologies are due to the growth of particular crystalline planes, which relies on the basic crystal facets affecting the FCC system, namely (100), (110), and (111) planes or a combination of them (for high-index facets). The role of the surface-regulating agents, which are in most cases added to the formulation in order to drive the growth of particular planes rather than others, is particularly interesting and intriguing. Obviously, different surface-regulating agents act on different planes. For instance, PVP (the capping agent that actually works as a surfactant) weakly interact with {100} facets of growing Ag nanostructure, thus slowing down their growth rate, and consequently favoring the formation of nanocubes or nanorods. Similar results are obtained by means of bromides. On the contrary, citrate (which is both a reductant and capping agent) preferentially interacts with {111} planes (here even slowing down their growth), thus favoring the formation of nanoplates.

Therefore, accordingly to the most recent results reported in the literature, a critical analysis of the driving forces (tips and tricks) at the basis of the formation of such particular nanostructures has been here discussed. The main outcomes justify the great attention given to the starting conditions of the synthesis, since the growth of the desired nanoscopic architecture is strongly affected by the first instants of the process. Interestingly, not only the type of capping agent is influencing the final morphology, but also other parameters (such as temperature, concentration of reactants, reaction time, pH, etc.) are matter of investigation by researchers with the aim of optimizing the desired structures. Surely, the exact role of each parameter is not always clear, and the differences among the several recipes, mostly, are so significant that linear correlations among the key-factors are hard to be found, thus making the process of production of such metallic nanoscopic architectures still empirical. However, even if several open questions are still present, such a critical review would hopefully shed light on many points. Lastly, in order to describe all the potentiality of the wet chemical methods for the production of particular exotic morphologies, several case studies suggested by the literature have been discussed and organized into three main subgroups: (i) triangular planes, (ii) branched structures (mostly nanostars and nanoflowers), and (iii) elongated structures (such as nanorods, nanowires, and filamentous nanonets). Particular emphasis has been devoted to the structure-influencing parameters, the critical points have been unveiled, and, when possible, the related growth mechanism has been proposed.

For all these reasons, the choice of the correct synthesis parameters is fundamental. In this review manuscript, a hopefully clear state-of-the-art overview which is provided to researchers and formulators, who can find useful guidelines for a correct aprioristic experimental design aimed to the synthesis of shape-controlled silver nanostructures.

Acknowledgements

Polytechnic of Torino is gratefully acknowledged for funding project Starting Grant RTD (project number: 54_RSG17NIR01).

Conflict of Interest

The authors declare no conflict of interest.

Keywords: silver nanoparticles · materials science · nanomaterials · nanotechnology · surface science

[1] C. Tan, X. Cao, X.-J. Wu, Q. He, J. Yang, X. Zhang, J. Chen, W. Zhao, S. Han, G.-H. Nam, M. Sindoro, H. Zhang, *Chem. Rev.* **2017**, *117*, 6225–6331.
[2] M. Auffan, J. Rose, J. Y. Bottero, G. V. Lowry, J. P. Jolivet, M. R. Wiesner, *Nat. Nanotechnol.* **2009**, *4*, 634–664.
[3] J. S. Duhan, R. Kumar, N. Kumar, P. Kaur, N. Nehra, S. Duhan, *Biotechnol. Rep.* **2017**, *15*, 11–23.
[4] M. A. Van Hove, *Catal. Today* **2006**, *113*, 133–140.
[5] M. S. Bakshi, *Adv. Colloid Interface Sci.* **2018**, *256*, 101–110.
[6] M. Mozetič, A. Vesel, G. Primc, C. Eisenmenger-Sittner, J. Bauer, A. Eder, G. H. S. Schmid, D. N. Ruzic, Z. Ahmed, D. Barker, K. O. Douglass, S. Eckel, J. A. Fedchak, J. Hendricks, N. Klimov, J. Ricker, J. Scherschligt, J. Stone, G. Strouse, I. Capan, M. Buljan, S. Milošević, C. Teichert, S. R. Cohen, A. G. Silva, M. Lehocky, P. Humpoliček, C. Rodriguez, J. Hernandez-Montelongo, D. Mercier, M. Manso-Silván, G. Ceccone, A. Galtayries, K. Stana-Kleinschek, I. Petrov, J. E. Greene, J. Avila, C. Y. Chen, B. Caja-Munoz, H. Yi, A. Boury, S. Lorcy, M. C. Asensio, J. Bredin, T. Gans, D. O'Connell, J. Brendin, F. Reniers, A. Vincze, M. Anderle, L. Montelius, *Thin Solid Films* **2018**, *660*, 120–160.
[7] E. Guihen, *TrAC Trends Anal. Chem.* **2013**, *46*, 1–14.
[8] L. Fan, B. Zhu, P.-C. Su, C. He, *Nano Energy* **2018**, *45*, 148–176.
[9] O. C. Farokhzad, R. Langer, *ACS Nano* **2009**, *3*, 16–20.
[10] L. Peng, B. L. Li, C. W. Zhou, N. B. Li, M. I. Setyawati, H. L. Zou, *Appl. Mater. Today* **2018**, *11*, 166–188.
[11] S. Chatterjee, F. Nafezarefi, N. H. Tai, L. Schlagenhauf, F. A. Nuesch, B. T. T. Chu, *Carbon* **2012**, *50*, 5380–5386.
[12] S. A. Jadhav, R. Nisticò, G. Magnacca, D. Scalarone, *RSC Adv.* **2018**, *8*, 1246–1254.
[13] H. Cabral, K. Miyata, A. Kishimura, *Adv. Drug Delivery Rev.* **2014**, *74*, 35–52.
[14] R. Nisticò, P. Avetta, P. Calza, D. Fabbri, G. Magnacca, D. Scalarone, *Beilstein J. Nanotechnol.* **2015**, *6*, 2105–2112.
[15] B. A. Krajina, A. C. Proctor, A. P. Schoen, A. J. Spakowitz, S. C. Heilshorn, *Progr. Mater. Sci.* **2018**, *91*, 1–23.
[16] R. Nisticò, *Res. Chem. Intermed.* **2017**, *43*, 6911–6949.
[17] G. Prieto, H. Tuysuz, N. Duyckaerts, J. Knossalla, G. -H. Wang, F. Schuth, *Chem. Rev.* **2016**, *116*, 14056–14119.
[18] R. Nisticò, D. Scalarone, G. Magnacca, *Microporous Mesoporous Mater.* **2017**, *248*, 18–29.
[19] S. Deville, *Scr. Mater.* **2018**, *147*, 119–124.
[20] R. Nisticò, G. Magnacca, M. Antonietti, N. Fechler, *Z. Anorg. Allg. Chem.* **2014**, *640*, 582–587.
[21] X. K. Meng, S. C. Tang, S. Vongehr, *J. Mater. Sci. Technol.* **2010**, *26*, 487–522.
[22] J. Zhang, Q. Kuang, Y. Jiang, Z. Xie, *Nano Today* **2016**, *11*, 661–677.
[23] H. Wei, H. Xu, *Nanoscale* **2013**, *5*, 10794–10805.
[24] Y. K. Mishra, N. A. Murugan, J. Kotakoski, J. Adam, *Vacuum* **2017**, *146*, 304–307.
[25] J. Soni, in: *Nanostructures for Novel Therapy, Synthesis, Characterization and Applications*, A volume in Micro and Nano Technologies, Eds: D. Ficai, A. M. Grumezescu, Elsevier, Amsterdam, Netherlands, **2017**, Ch. 25.
[26] J. R. Nakkala, R. Mata, S. R. Sadras, *J. Colloid Interface Sci.* **2017**, *499*, 33–45.
[27] C. Novara, A. Lamberti, A. Chiadò, A. Virga, P. Rivolo, F. Geobaldo, F. Giorgis, *RSC Adv.* **2016**, *6*, 21865–21870.
[28] N. Kalfagiannis, P. G. Karagiannidis, C. Pitsalidis, N. T. Panagiotopoulos, C. Gravalidis, S. Kassevetis, P. Patsalas, S. Logothetidis, *Sol. Energy Mater. Sol. Cells* **2012**, *104*, 165–174.
[29] J. Fang, S. Liu, Z. Li, *Biomaterials* **2011**, *32*, 4877–4884.
[30] T. Tsuji, M. Kikuchi, T. Kagawa, H. Adachi, M. Tsuji, *Colloids Surf. A* **2017**, *529*, 33–37.
[31] R. Nisticò, M. Barrasso, G. A. Carrillo Le Roux, M. M. Seckler, W. Sousa, M. Malandrino, G. Magnacca, *ChemPhysChem* **2015**, *16*, 3902–3909.

[32] X. Guo, D. Deng, Q. Tian, C. Jiao, *Adv. Powder Technol.* **2014**, *25*, 865–870.
[33] Y. N. Wijaya, J. Kim, W. M. Choi, S. H. Park, M. H. Kim, *Nanoscale* **2017**, *9*, 11705–11712.
[34] A. Garcia-Leis, I. Rivera-Arreba, S. Sanchez-Cortes, *Colloids Surf. A* **2017**, *535*, 49–60.
[35] G. Qingquan, M. Xinfu, X. Yu, T. Wei, Z. Hui, *Colloids Surf. A* **2017**, *530*, 33–37.
[36] P. S. Mdluli, N. Reveprasadu, *Mater. Lett.* **2009**, *63*, 447–450.
[37] G. Wu, S. Yang, Q. Liu, *Appl. Surf. Sci.* **2015**, *357*, 583–592.
[38] Y.-C. Hsu, Y.-M. Chen, W.-L. Lin, Y.-F. Lan, Y.-N. Chan, J.-J. Lin, *J. Colloid Interface Sci.* **2010**, *352*, 81–86.
[39] D. E. Sands, *Introduction to Crystallography*, Dover Publication Inc., Mineola, New York, **1993**.
[40] G. D. Barmparis, Z. Lodziana, N. Lopez, I. N. Remediakis, *Beilstein J. Nanotechnol.* **2015**, *6*, 361–368.
[41] J. -F. Ganghoffer, in: *Thermodynamics - Interaction Studies - Solids, Liquids and Gases*, Ed.: J. C. Moreno Pirajan, IntechOpen Limited, London, UK, **2011**, Ch.14.
[42] X. Xia, J. Zeng, L. K. Oetjen, Q. Li, Y. Xia, *J. Am. Chem. Soc.* **2012**, *134*, 1793–1801.
[43] L. D. Marks, L. Peng, *J. Phys. Condens. Matter* **2016**, *28*, 053001.
[44] P. Zhang, I. Wyman, J. Hu, S. Lin, Z. Zhong, Y. Tu, Z. Huang, Y. Wei, *Mater. Sci. Eng. B* **2017**, *223*, 1–23.
[45] S. Gómez-Grana, B. Goris, T. Altantzis, C. Fernández-López, E. Carbó-Argibay, A. Guerrero-Martínez, N. Almora-Barrios, N. López, I. Pastoriza-Santos, J. Pérez-Juste, S. Bals, G. Van Tendeloo, L. M. Liz-Marzán, *J. Phys. Chem. Lett.* **2013**, *4*, 2209.
[46] X. Xia, J. Zeng, B. McDearmon, Y. Zheng, Q. Li, Y. Xia, *Angew. Chem. Int. Ed.* **2011**, *50*, 12542–12546; *Angew. Chem.* **2011**, *123*, 12750–12754.
[47] N. L. Pacioni, C. D. Borsarelli, V. Rey, A. V. Veglia, in: *Silver Nanoparticle Applications, In the Fabrication and Design of Medical and Biosensing Devices, Engineering Materials,* Eds: E. I. Alarcon, M. Griffith, K. I. Udekwu, Springer International Publishing, Basel, Switzerland, **2015**, Ch. 2.
[48] J. Turkevich, P. C. Stevenson, J. Hillier, *Discuss. Faraday Soc.* **1951**, *11*, 55–75.
[49] R. Nisticò, A. Rosellini, P. Rivolo. M. G. Faga, R. Lamberti, S. Martorana, M. Castellino, A. Virga, P. Mandracci, M. Malandrino, G. Magnacca, *Appl. Surf. Sci.* **2015**, *328*, 287–295.
[50] J. Polte, X. Tuaev, M. Wuithschick, A. Fischer, A. F. Thuenemann, K. Rademann, R. Kraehnert, F. Emmerling, *ACS Nano* **2012**, *6*, 5791–5802.
[51] Z. S. Pillai, P. V. Kamat, *J. Phys. Chem. B* **2004**, *108*, 945–951.
[52] S. T. Gentry, S. F. Kendra, M. W. Bezpalko, *J. Phys. Chem. C* **2011**, *115*, 12736–12741.
[53] D. Palma, A. Bianco Prevot, L. Celi, M. Martin, D. Fabbri, G. Magnacca, M. R. Chierotti, R. Nisticò, *Catalysts* **2018**, *8*, 197.
[54] R. Nisticò, *Beilstein J. Nanotechnol.* **2018**, *9*, 2332–2344.
[55] Y. Chen, Y. Chen, P. Hu, S. Ma, Y Li, *Ceram. Int.* **2016**, *42*, 18516–18520.
[56] N. J. Turro, P. L. Kuo, *J. Phys. Chem.* **1986**, *90*, 837–841.
[57] M. Antonietti, *Curr. Opin. Colloid Interface Sci.* **2001**, *6*, 244–248.
[58] Y. Sun, B. Mayers, T. Herricks, Y. Xia, *Nano Lett.* **2003**, *3*, 955–960.
[59] B. Wiley, Y. Sur, B. Mayers, Y. Xia, *Chem. Eur. J.* **2005**, *11*, 454–463.
[60] Y.-Y. Yu, S.-S. Chang, C.-L. Lee, C. R. C. Wang, *J. Phys. Chem. B* **1997**, *101*, 6661–6664.
[61] X. Huang, Z. Zhao, J. Fan, Y. Tan, N. Zheng, *J. Am. Chem. Soc.* **2011**, *133*, 4718–4721.
[62] O. A. Oviedo, P. Velez, V. A. Macagno, E. P. M. Leiva, *Surf. Sci.* **2015**, *631*, 23–34.
[63] Y. V. Bokshits, N. P. Osipovich, E. A. Strel'tsov, G. P. Shevchenko, *Colloids Surf. A* **2004**, *242*, 79–83.
[64] M. L. Personick, M. R. Langille, J. Zhang, C. A. Mirkin, *Nano Lett.* **2011**, *11*, 3394–3398.
[65] H.-X. Lin, Z.-C. Lei, Z.-Y. Jiang, C.-P. Hou, D.-Y. Liu, M.-M. Xu, Z.-Q. Tian, Z.-X. Xie, *J. Am. Chem. Soc.* **2013**, *135*, 9311–9314.
[66] Q. H. Tran, V. Q. Nguyen, A.-T. Le, *Adv. Nat. Sci.: Nanosci. Nanotechnol.* **2013**, *4*, 033001.
[67] L. Rodriguz-Sanchez, M. C. Blanco, M. A. Lopez-Quintela, *J. Phys. Chem. B* **2000**, *104*, 9683–9688.
[68] H.-H. Park, X. Zhang, Y.-J. Choi, H.-H. Park, R. H. Hill, *J. Nanomater.* **2011**, *2011*, 265287.
[69] I. Ghiuta, D. Cristea, C. Croitoru, J. Kost, R. Wenkert, I. Vyrides, A. Anayiotos, D. Munteanu, *Appl. Surf. Sci.* **2018**, *438*, 66–73.
[70] I. Maliszewska, K. Szewczyk, K. Waszak, *J. Phys. Conf. Ser.* **2009**, *146*, 012025.
[71] C. Wang, B. Liu, X. Dou, *Sens. Actuators B* **2016**, *231*, 357–364.
[72] B. Xue, D. Wang, J. Zuo, X. Kong, Y. Zhang, X. Liu, L. Tu, Y. Chang, C. Li, F. Wu, Q. Zeng, H. Zhao, H. Zhao, H. Zhang, *Nanoscale* **2015**, *7*, 8048–8057.
[73] H. Jia, W. Xu, J. An, D. Li, B. Zhao, *Spectrochim. Acta Part A* **2006**, *64*, 956–960.
[74] K. Li, X. Jia, A. Tang, X. Zhu, H. Meng, Y. Wang, *Integr. Ferroelectr.* **2012**, *136*, 9–14.
[75] Q. Zhang, N. Li, J. Goebl, Z. Lu, Y. Yin, *J. Am. Chem. Soc.* **2011**, *133*, 18931–18939.
[76] T. Zang, Y.-J. Song, X.-Y. Zhang, J.-Y. Wu, *Sensors* **2014**, *14*, 5860–5889.
[77] A. Shioara, S. M. Novikov, D. M. Solis, J. M. Taboada, F. Obellero, L. M. Liz-Marzan, *J. Phys. Chem. C* **2015**, *119*, 10836–10843.
[78] A. Shiohara, Y. Wang, L. M. Liz-Marzan, *J. Photochem. Photobiol. C* **2014**, *21*, 2–25.
[79] Y. Wang, P. H. C. Camargo, S. E. Skrabalak, H. Gu, Y. Xia, *Langmuir* **2008**, *24*, 12042–12046.
[80] X. W. Lou, C. Yuan, L. A. Archer, *Chem. Mater.* **2006**, *18*, 3921–3923.
[81] B. K. Jena, B. K. Mishra, S. Bohidar, *J. Phys. Chem. C* **2009**, *113*, 14753–14758.
[82] C.-Y. Zhang, R. Hao, B. Zhao, Y.-Z. Fu, Y.-W. Hao, Y.-Q. Liu, *J. Mater. Sci.* **2017**, *52*, 11391–11401.
[83] Z. Zhong, D. Wang, Y. Cui, M. W. Bochrath, C. M. Lieber, *Science* **2003**, *302*, 1377–1379.
[84] C. Chen, L. Wang, H. Yu, G. Jiang, Q. Yang, J. Zhou, W. Xiang, J. Zhang, *Mater. Chem. Phys.* **2008**, *107*, 13–17.
[85] G.-J. Lee, S.-I. Shin, Y.-C. Kim, S.-G. Oh, *Mater. Chem. Phys.* **2004**, *84*, 197–204.
[86] J. M. Petroski, Z. L. Wang, T. C. Green, M. A. El-Sayed, *J. Phys. Chem. B* **1998**, *102*, 3316–3320.
[87] A. Filankembo, S. Giorgio, I. Lisiecki, M. P. Pileni, *J. Phys. Chem. B* **2003**, *107*, 7492–7500.
[88] R. Nisticò, S. Tabasso, G. Magnacca, T. Jordan, M. Shalom, N. Fechler, *Langmuir* **2017**, *33*, 5213–5222.
[89] C.-L. Lee, C.-M. Syu, *Colloids Surf. A* **2010**, *358*, 158–182.

Manuscript received: January 8, 2019
Revised manuscript received: March 10, 2019